Role of stoichiometry and implicit negative feedback in sigma factor regulation

Jatin Narula[a], Abhinav Tiwari[a] and Oleg A. Igoshin[a,1]

[a]Department of Bioengineering, Rice University, Houston, TX 77005;

[1]To whom correspondence should be addressed. Email: igoshin@rice.edu

Major Subject Areas: Computational and systems biology, Microbiology & Infectious disease

Keywords: stress response, sigma factor, pulse regulation, feedback loops, ultrasensitivity

Research Organism: *Bacillus subtlis*

Abstract

Despite the central role of alternative sigma factors in bacterial stress response and virulence their regulation remains poorly understood. Here we investigate one of best-studied examples of alternative sigma factors: the σ^B network that controls the general stress response of *Bacillus subtilis* to uncover widely relevant general design principles that describe the structure-function relationship of alternative sigma factor regulatory networks. We show that the relative stoichiometry of the synthesis rates of σ^B, its anti-sigma factor RsbW and the anti-anti-sigma factor RsbV, plays a critical role in shaping the network behavior by forcing the σ^B network to function as an ultrasensitive negative feedback loop. We further demonstrate how this type of negative feedback regulation insulates alternative sigma factor activity from competition with the housekeeping sigma factor for RNA polymerase and allows multiple stress sigma factors to function simultaneously with little competitive interference.

Introduction

Bacteria survive in stressful environmental conditions by inducing dramatic changes in their gene expression patterns (1, 2). For a variety of stresses, these global changes in gene expression are brought about by the activation of alternative sigma factors that bind the RNA polymerase core enzyme and direct it towards the appropriate stress response genes (3). The ability of these alternative sigma factors to capture core-RNA polymerase and direct the expression of their stress regulon is determined by their free concentrations and affinity for core-RNA polymerase (4). Consequently, to ensure that these sigma factors are only active under specific environmental conditions, bacteria have evolved regulatory systems to control their production, activity and availability (3, 5). These regulatory networks can be highly complex but frequently share features such as anti-sigma factors, partner switching mechanisms and proteolytic activation (5). The complexity of these networks has prevented the development of a clear mechanistic understanding of their structure-function relationship. In this study, we focus on one of the best studied examples of alternative sigma factors, the general stress-response regulating σ^B in *Bacillus subtilis* (6) to understand how the structure of the sigma factor regulatory networks is related to their functional response.

The σ^B-mediated response is triggered by diverse energy and environmental stress signals and activates expression of a broad array of genes needed for cell survival in these conditions (6). σ^B activity is tightly regulated by a partner-switching network (Fig. 1A) comprising σ^B, its antagonist anti-sigma factor RsbW, and anti-anti-sigma factor RsbV. In the absence of stress, RsbW dimer ($RsbW_2$) binds to σ^B and prevents its association with RNA polymerase thereby turning OFF the σ^B regulon. Under these conditions $RsbW_2$ inactivates most of RsbV by using its kinase activity to phosphorylate RsbV. The phosphorylated form of RsbV (RsbV~P) has a low affinity for $RsbW_2$ and cannot interact with it effectively (7). However, in the presence of stress, RsbV~P is dephosphorylated by one or both of the dedicated phosphatases, RsbQP for energy stress and RsbTU for environmental stress (8-11). Dephosphorylated RsbV attacks the σ^B-$RsbW_2$ complex to induce σ^B release, thereby turning ON the σ^B regulon (12). Notably, the genes encoding σ^B and its regulators lie within a σ^B-controlled operon (13), thereby resulting in positive and negative feedback loops.

Recently, it was shown that under energy stress σ^B is activated in a stochastic series of transient pulses and increasing stress resulted in higher pulse frequencies (14). It has also been shown that increase in environmental stressor such as ethanol leads to a single σ^B pulse with an amplitude that is sensitive to the rate of stressor increase (15). While it is clear that the pulsatile activation of σ^B is rooted in the complex architecture of its regulatory network (Fig. 1A) its mechanism is not fully understood. Previous

mathematical models of the σ^B network either did not produce the pulsatile response (16) or made ad hoc simplifications to the network (14) that are somewhat inconsistent with experimentally observed details. As a result, it remains unclear which design features of the σ^B network enable its functional properties.

To address these issues we develop a detailed mathematical model of the σ^B network and examine its dynamics to understand the mechanistic principles underlying the pulsatile response. By decoupling the post-translational and transcriptional components of the network we show that an ultrasensitive negative feedback between the two is the basis for σ^B pulsing. Moreover we find that the relative stoichiometry of σ^B, RsbW and RsbV synthesis rates plays a critical role in determining the qualitative nature of the σ^B response. We also use our model, together with experimental data, to explain how the σ^B network is able to encode the rate of stress increase and the size of stochastic bursts of stress phosphatase into the amplitudes of σ^B pulses.

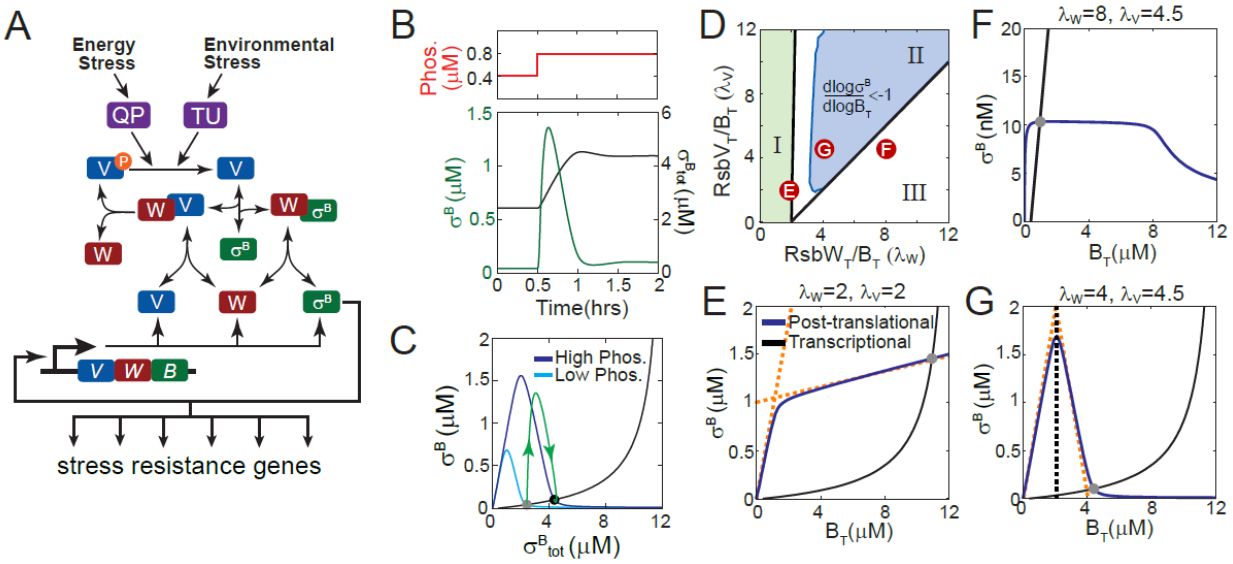

Figure 1. σ^B general stress response network. A. Network diagram of the σ^B general stress response. Energy and environmental stresses activate the stress-sensing phosphatases RsbQP (QP) and RsbTU (TU) which dephosphorylate RsbV which in turn activates σ^B by releasing it from the σ^B-$RsbW_2$ complex. **B.** Dynamics of free σ^B and B_T in response to a step-increase in phosphatase concentration. **C.** Representation of the σ^B pulsatile trajectory in (B) in the σ^B-B_T phase plane (green curve). Blue and cyan curves show the decoupled post-translational response at high and low phosphatase respectively. The black curve shows the transcriptional response. **D.** (λ_W, λ_V) stoichiometry parameter space divided into three Regions (I, II, III) corresponding to differences in sign of the σ^B network feedback and response. Positive feedback in Region I, negative feedback in Region II (ultrasensitive in blue sub-region) and non-responsive in Region III (free σ^B is always low). Red circles mark the selected values of (λ_W, λ_V)

used in panels E-G. **E-G.** Simplified view of the decoupled post-translational and transcriptional components of the σ^B network in Regions I-III. Blue and black curves show the post-translational and transcriptional responses respectively. Gray circles mark the steady states of the full system. Dashed orange curves show linear asymptotic approximations of the post-translational response (see text). The dashed vertical line in (G) shows the critical level of operon expression beyond which free σ^B decreases as a function of B_T.

We further develop this model to investigate how the network functions in the context of other sigma factors. As in many other bacteria, σ^B is one of the many sigma factors that complex with RNA-polymerase core that is present in limited amounts (3, 17). Therefore, when induced these alternative sigma factors compete with one another and the housekeeping sigma factor σ^A for RNA polymerase. We use our model to investigate how the design of this network enables it to function even in the presence of competition from σ^A which has a significantly higher affinity for RNA polymerase (18). Lastly, we investigate how multiple alternative sigma factors cross-talk and compete when cells are exposed to multiple stresses simultaneously. Using our model we identify design features that are ubiquitous in stress sigma factor regulation and critical to bacterial survival under diverse types of stresses.

Results

Biochemically accurate model of σ^B pulsing

In a recent study, Locke et. al. (14) demonstrated that a step-increase in energy stress results in pulsatile activation of σ^B. The study also proposed a minimal mathematical model of the network which reproduced pulsing in σ^B. However, this model included several ad hoc assumptions: (i) Phosphorylation and dephosphorylation reactions were assumed to follow Michaelis-Menten kinetics despite the fact that kinase (RsbW) and phosphatase concentrations are known to be comparable to substrate (RsbV) concentrations (19), (ii) σ^B and RsbV are represented as a single lumped variable rather than separate species and, (iii) partner-switching, and the formation and dissociation of various $RsbW_2$ complexes were not included explicitly. Though this minimal model produces pulses resembling their experimental observations, it does not depict a biochemically accurate picture of the σ^B network. Consequently it cannot be used to uncover the design features that enable σ^B pulsing.

To understand the σ^B network response we built on our earlier study (16) to develop a detailed mathematical model that explicitly includes all known molecular interactions in the network. We note that we made one significant change to the model discussed in

(16). The model in (16) assumed that the synthesis rates for total σ^B and its network partners (RsbW and RsbV) follow their stoichiometric binding ratios (i.e. $W_T/B_T = \lambda_W = 2$ and $V_T/B_T = \lambda_V = 2$). In contrast, here following the experimental measurements of (19), we assumed that σ^B, RsbW and RsbV are produced in non-stoichiometric ratios ($\lambda_W = 4$ and $\lambda_V = 4.5$). Simulations of this detailed model showed that it is able to reproduce the experimentally observed response. Specifically, we found that a step-increase in phosphatase concentration led to an increase in free σ^B followed by an increase in the total σ^B concentration (B_T) (Fig. 1B). Thereafter free σ^B levels decreased thus exhibiting the pulsatile response observed in the experiments of Locke et. al. (14).

To understand this pulsatile response, we decouple the network's transcriptional and post-translational responses in our model. By varying the σ^B operon transcription rate, while keeping the ratio of operon component synthesis rates (λ_W, λ_V) fixed we were able to calculate the post-translational response of the σ^B network: $\sigma^B = F_P(B_T, P_T)$. This function describes how the concentration of free σ^B varies as a function of total σ^B concentration (B_T) and total phosphatase concentration (P_T). In parallel, we calculated the transcriptional response $B_T = F_T(\sigma^B)$, describing how changes in free σ^B concentration affect the total σ^B concentrations (RsbW and RsbV concentrations are proportional to B_T). In this analysis framework, the steady state of the complete closed loop network can be determined by simultaneously solving the post-translational and transcriptional functions, $\sigma^B = F_P(B_T, P_T)$ and $B_T = F_T(\sigma^B)$, for σ^B and B_T for each phosphatase concentration P_T. P_T controls this steady state via its role in the post-translational response function $F_P(B_T, P_T)$.

The effective sign of the feedback in the σ^B network is given by the product of the sensitivities $(\partial F_T/\partial \sigma^B)*(\partial F_P/\partial B_T)$. Since sigma factors function as activators of transcription, $F_T(\sigma^B)$ is a monotonically increasing function of σ^B (i.e. $\partial F_T/\partial \sigma^B > 0$). Consequently, the sign of the feedback in the σ^B network is given by the sign of the sensitivity of the post-translational response to B_T (i.e. $\partial F_P/\partial B_T$). Our results show that for the chosen parameters F_P is a non-monotonic function of B_T (Fig. 1C). At low B_T, free σ^B increases as a function of B_T because RsbW is sequestered in the W_2V_2 complex. However at higher B_T, the kinase flux dominates the phosphatase flux and the anti-sigma factor dimer $RsbW_2$ sequesters σ^B in the $W_2\sigma^B$ complex such that free σ^B decreases ultrasensitively as a function of B_T. In this regime the feedback loop between σ^B amount and activity is negative. Notably, negative feedback is one of the few network motifs that is known to be capable of producing adaption-like pulsatile responses (20). This explains how a step-increase in the phosphatase concentration in our model simulations leads to a σ^B pulse. Plotting the trajectory of the σ^B pulse on the (σ^B, B_T) plane over the post-translational and transcriptional responses (Fig. 1C) illustrates the mechanism driving this pulsatile response. Starting at the initial steady state, an

increase in phosphatase shifts the ultrasensitive post-translational response so that free σ^B is rapidly released from the $W_2\sigma^B$ complex whereas B_T remains relatively unchanged. Once the free σ^B level matches the post-translational response it stops increasing. The increase in σ^B operon transcription eventually causes accumulation of B_T (and the anti-sigma factor RsbW). This in turn forces the σ^B level to decrease, following the post-translational response curve, to the new steady state which has very little free σ^B thereby completing the σ^B pulse.

These new insights into the pulsing mechanism facilitates the identification of critical design features required for pulsing. For example, these results explain why pulsing does not occur in strains in which σ^B operon is transcribed constitutively (14). In this case, the σ^B network lacks the negative feedback necessary to produce a pulsatile response. A step-increase in phosphatase still leads to an increase in free σ^B due to the change in the post-translational response, however, this not followed by an increase in B_T (Fig. S1A). Consequently, an increase in phosphatase results in a monotonic increase in free σ^B rather than a pulse (Fig. S1A).

Our decoupling method also sheds light on the dependence of σ^B pulse amplitude on the phosphatase level and transcriptional and post-translational model parameters. Specifically, we found that σ^B pulse amplitude is a threshold-linear function of the phosphatase concentration (Fig. S2A). Below the phosphatase threshold, the post-translational response $\sigma^B=F_P(B_T, P_T)\sim=0$ and is insensitive to B_T (Fig. S2B). Thus, the full system lacks the negative feedback and as a result σ^B does not pulse. Above the threshold, σ^B pulse amplitudes increase linearly as a function of phosphatase concentration. Our results further show that both the phosphatase threshold and sensitivity of pulse amplitudes to above-threshold phosphatase depend on post-translational parameters that control the ultrasensitivity of the post-translational response, specifically the ratio of the phosphatase and kinase catalytic rate constants (k_p/k_k) (Fig. S2B) and binding affinity of σ^B and RsbV for the $RsbW_2$ dimer (Fig. S2C).

σ^B response dynamics depend on operon relative stoichiometry

Next we further investigated the post-translational response of the σ^B network and found that the ratio of the synthesis rates of operon components ($\lambda_{W=} W_T/B_T$, $\lambda_{V=} V_T/B_T$) plays a critical role in determining both qualitative and quantitative features of $\sigma^B = F_P(B_T,P_T)$. As shown in Fig. 1D, the (λ_W, λ_V) parameter space can be divided into three regions based on qualitative differences in the post-translational response.

In Region I, the amount of RsbW, irrespective of P_T, is insufficient to bind all of its partners. Consequently, a fraction of B_T always exists as free σ^B. As a result, sensitivity

of free σ^B concentrations to B_T is positive ($dF_P/dB_T > 0$) for all phosphatase concentrations. In contrast, in Region II, whether the amount of RsbW is sufficient to bind all of its partners depends on how much RsbV is in its inactive phosphorylated form RsbV~P (V_P). As a result, for this region, the ratio of total kinase W_T ($=\lambda_W B_T$) and total phosphatase P_T determines the post-translational dependence of free σ^B concentrations to B_T. At low W_T/P_T, V is unphosphorylated and free σ^B concentrations increases as a function of B_T ($dF_P/dB_T > 0$), but at high W_T/P_T, V is mostly in its phosphorylated form and free σ^B concentrations decreases as a function of B_T ($dF_P/dB_T < 0$). Region III is the opposite of Region I in that the amount of RsbW, is more than sufficient to bind all of its partners, even when all V is unphosphorylated. Consequently, irrespective of P_T levels, very little σ^B is free and its level is insensitive to changes in B_T ($dF_P/dB_T \sim 0$). Figures 1E-G illustrate the different post-translational responses in the three regions for three selected combinations (red circles in Figure 1D) of stoichiometric ratios (λ_W, λ_V).

The boundaries of these three regions and the post-translational response within them can be clearly determined if σ^B and its partners bind strongly to each other. Since this is indeed the case for the σ^B network, we can assume that all species in the network exist in their respective complexed forms. Using this assumption we found that the post-translational response of the network is defined by critical level of kinase W_0 ($=2k_pP_T/k_k$). Intuitively, W_0 corresponds to the concentration of RsbW at which maximal kinase flux is equal maximal phosphatase flux and thus it is a function of phosphatase level and the catalytic rate constants of the kinase (k_k) and phosphatase (k_p) catalytic steps. When total kinase level is below this critical threshold ($W_T<W_0(P_T)$), phosphatase flux dominates and V exists mostly in its unphosphorylated form. In contrast, for $W_T>W_0(P_T)$, kinase flux starts dominating and therefore V_P accumulates in a kinase-concentration dependent manner. Taking this into account, it can be shown that this post-translational dependence of free σ^B on B_T (proportional to total kinase W_T) can be approximately described by the following equations (see Supplementary Text for derivation):

$$\sigma^B = \begin{cases} B_T\left(1+(\lambda_V-\lambda_W)/2\right) & B_T < W_0(P_T)/\lambda_W \\ B_0(P_T) - B_T\left(\lambda_W/2 - 1 - \lambda_V k_{deg}/k_k\right) & B_T \geq W_0(P_T)/\lambda_W \end{cases}$$

Where k_{deg} represents the rate constant for degradation ($<<k_k$). Note that this equation provides a close approximation for the post-translational response of the σ^B network in different regions of the (λ_W, λ_V) parameter space (Fig. 1EF, dashed lines). Further this asymptotic description of the post-translational response can identify the boundaries of Regions I-III. Specifically we found that $d\sigma^B/dB_T$ is always positive for ($\lambda_W <= 2 + \lambda_V k_{deg}/k_k$) – which therefore defines Region I. Further for ($2 + \lambda_V k_{deg}/k_k < \lambda_W < \lambda_V + 2$), the

sign of $d\sigma^B/dB_T$ depends on P_T, which is characteristic of Region II. Finally Region III is defined by $\lambda_W > \lambda_V + 2$, where RsbW exceeds all of its partners and $\sigma^B/B_T \sim 0$.

Notably, since σ^B always increases as a function of B_T in Region I and since σ^B transcriptionally activates B_T production, a positive feedback exists in the σ^B network in this region. Similarly since ($dF_P/dB_T \sim 0$), in Region III the network is non-responsive in this Region. As a result, step-increases in phosphatase concentration in Regions I and III of the (λ_W, λ_V) parameter space do not produce σ^B pulse (Fig. S1BC). This absence of pulsing can be explained by the lack of negative feedback in these regions. Thus our model shows that the relative stoichiometry of σ^B operon expression rates and post-translational sensitivity of σ^B to operon expression levels play a critical role in determining the qualitative nature of the σ^B response. In the following sections, we used our model to further investigate the design-function relationship of the σ^B network.

Under energy stress conditions σ^B network encodes phosphatase burst size into pulse amplitudes

Thus far we have shown how the σ^B network responds to a step-increase in phosphatase by producing a single pulse of activity. However, in a recent study Locke et. al. (14) have shown that an increase in energy stress leads to a sustained response with a series of stochastic pulses in σ^B activity. This study further showed that this sustained pulsing response is driven by noisy fluctuations in level of energy-stress-specific phosphatase RsbQP. While the mean level of RsbQP level is regulated transcriptionally by energy stress (9, 14), it's concentration in single cells can be noisy and fluctuate due to the stochasticity of gene expression. To determine if our model could explain this response to stochastic fluctuations in RsbQP, we modified our model to include noise in the concentration of this phosphatase.

Based on previous theoretical (21, 22) and experimental (23) studies we assume that this fluctuating phosphatase level follows a gamma distribution which is described by two parameters - burst size (*b*, average number of molecules produced per burst) and burst frequency (*a*, number of bursts per cell cycle). The mean phosphatase in this case is the product of burst size and burst frequency ($\langle P_T \rangle = ab$). Thus, stress can increase mean phosphatase by either changing burst size or burst frequency.

From the results of (14) it is unclear whether the increase in phosphatase at high stress is the result of increased mean burst size or burst frequency. First, we performed stochastic simulations in which mean phosphatase concentration was varied by changing burst size. These simulations showed that it is able to reproduce all the experimentally-observed features of the σ^B pulsatile response. Specifically our results

show that stochastic bursts in stress phosphatase levels lead to pulses of σ^B activity (Fig. 2A). Moreover, consistent with the experimental observations of (14), our model showed that the amplitude of σ^B pulses is a linear function of the stress phosphatase level (Fig. 2B). Finally we found that stress-mediated increases in phosphatase concentration lead to an increase in the frequency of σ^B pulsing (Fig. 2C) and an ultrasensitive increase in the level of σ^B target expression (Fig. 2D).

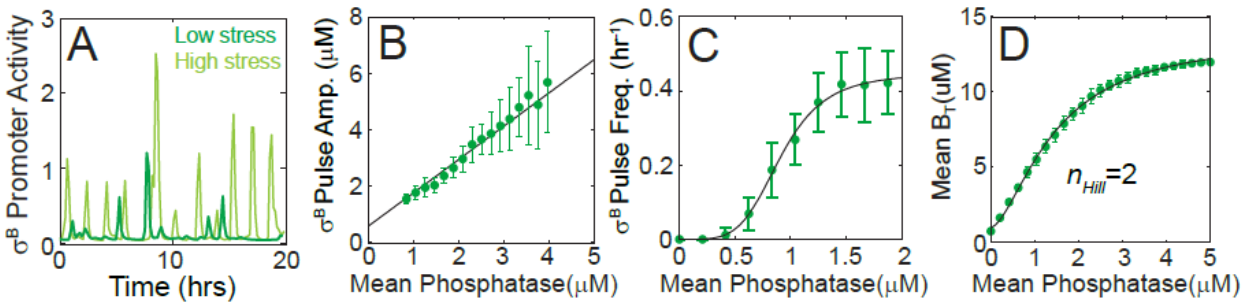

Figure 2. Pulsatile response of the σ^B network to stochastic phosphatase bursts during energy stress. A. Simulations of the detailed σ^B network model show that stochastic bursts in energy stress-sensing phosphatases RsbQP levels lead to pulses of σ^B target promoter activity. Light and dark green curves show sample trajectories from stochastic simulation at high and low stress respectively. **B.** σ^B pulse amplitudes increase linearly as a function of mean phosphatase level. Green circles and errorbars show mean and standard deviations calculated from stochastic simulations. Black line shows a linear fit. **C.** σ^B pulse frequency increases ultrasensitively as a function of mean phosphatase level. Green circles show the mean pulse frequency calculated from stochastic simulations. Black curve shows a Hill-equation fit with n_{Hill}=5.6. **D.** Mean σ^B target expression increases ultrasensitively as a function of mean phosphatase level. Green curves show the mean σ^B target expression calculated from stochastic simulations. Black curve shows a Hill-equation fit with n_{Hill} = 2.

Stochastic simulations of the σ^B network where mean phosphatase concentration was varied by changing burst frequency also led to an increase in σ^B pulsing. A key difference was that σ^B pulse amplitude increases ~5-fold for burst size modulation (Fig. 2B), whereas it remains constant for burst frequency modulation (Fig. S3A). Additionally, we found that in the case of burst size the increase in σ^B pulse frequency is non-linear, whereas in the case of burst frequency the increase is linear (compare Figs. 2C and S3B). Both burst size and burst frequency modulation led to a non-linear increase in the level of σ^B target expression (Figs. 2D and S3C). Notably the experimental observations reported in (14) show that σ^B pulse amplitude does increase (~3-fold) with an increase in energy stress thus suggesting that increase in phosphatase concentration at high stress is primarily the result of increase in burst size.

To further reinforce the role of mean burst size modulation in controlling the σ^B pulse response we next examined the cumulative histograms of pulse amplitudes at different phosphatase concentrations. These histograms carry different signatures for burst size or burst frequency encoding. Our results show that the distribution of pulse amplitudes is unchanged with increase in burst frequency (Fig. S3D). This is because the distribution of phosphatase burst sizes does not change when burst frequency is increased. In contrast, if phosphatase levels are controlled by changing mean burst size then the distribution of phosphatase burst size changes and so does the distribution of pulse amplitudes (Fig. S3E). Consequently, the normalized cumulative histograms of pulse amplitudes overlap for burst frequency encoding but not for burst size encoding. Applying this test to the data from (14), we found that in fact the normalized cumulative pulse amplitudes histograms do not overlap (Fig. S3F). These results confirm that the σ^B network adopts the mean burst size modulation strategy and encodes phosphatase burst size into σ^B pulse amplitudes.

σ^B network encodes rate of environmental stress increase into pulse amplitudes

We also used our model to study the response of the σ^B network to changes in environmental stress. Unlike the energy stress phosphatase, the environmental stress phosphatase RsbU is regulated post-translationally activated by binding of RsbT (24-26). Under unstressed conditions, RsbT is trapped by its negative regulators but it is released upon stress. Consequently, the concentration of RsbTU complex is tightly controlled on posttranslational level and therefore expected to be relatively insensitive to the effects stochastic gene expression fluctuations but depend on the level of environmental stress. As a result, step-up increases in environmental stress agents like ethanol produces rapid increase in RsbTU and result in only a single pulse of σ^B activity (15). However it has been shown that for gradual increases in stress, σ^B pulse amplitude depends on the rate of stress increase (15). To explain this response, we modeled gradual stress with ramped increase in RsbTU complex concentration (Fig. 3A). Our simulations showed that the detailed model is indeed able to capture the effect of rate of stress increase on σ^B pulse amplitudes. Specifically for a fixed RsbTU complex increase, the pulse amplitudes decrease non-linearly as a function of duration of the phosphatase ramp (Fig. 3B, E).

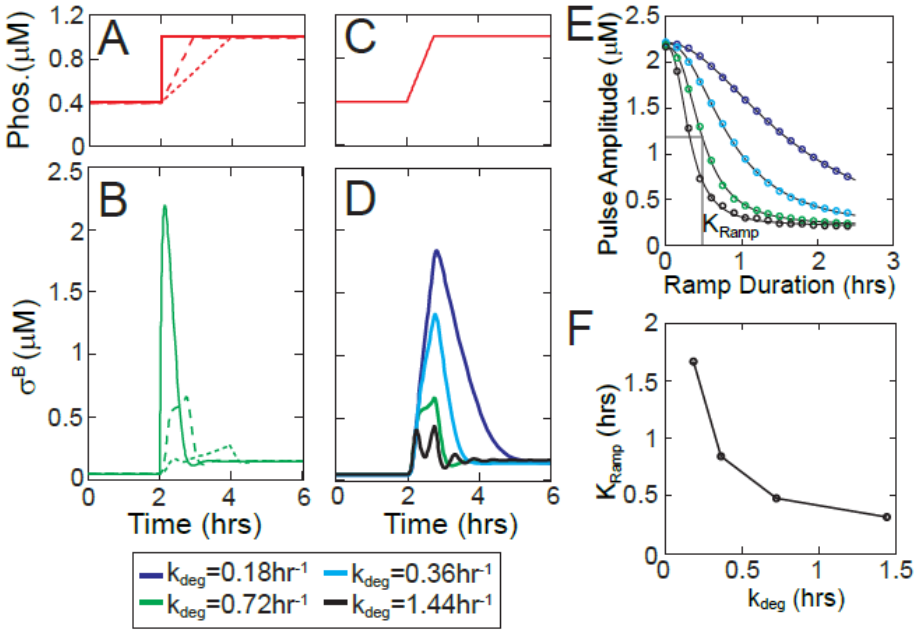

Figure 3. Rate sensitivity of the σ^B pulsatile response to environmental stress. A. Ramped increases in RsbTU complex concentration used as model inputs for σ^B network to simulate different rates of stress increase. **B.** σ^B pulse amplitudes in the wildtype model (k_{deg} = 0.72 hr^{-1}) resulting from the ramped increases in phosphatase concentration shown in (A). Note that the pulse amplitude decreases as phosphatase ramp durations increase. **C,D.** σ^B pulse amplitudes resulting from the ramped increase in phosphatase concentration shown in (C) for various degradation/dilution rates (D). Note that the pulse amplitudes decrease as degradation/dilution rates (k_{deg}) increase. **E.** Non-linear dependence σ^B pulse amplitudes on phosphatase ramp duration for various values of k_{deg}. The half-maximal constant of this dependence, K_{ramp} increases as k_{deg} decreases. Circles and solid curves represent simulation results and Hill-equation fits respectively. Colors represent different k_{deg} values as in (D). **F.** K_{ramp}, the half-maximal constant of the non-linear dependence of amplitudes on ramp durations, as a function of k_{deg}.

We hypothesized that this ramp rate encoding is the result of the timescale separation between the fast post-translational and the slow transcriptional responses of the σ^B network. During the pulsed σ^B activation, post-translational response is rate-limited by the phosphatase ramp. In contrast, the transcriptional response is slow and its rate is set by the degradation rate of σ^B operon proteins. For a step-increase in phosphatase the fast post-translational response ensures that σ^B reaches its post-translational steady state before the slow increase in RsbW sequesters σ^B and turn off the pulse (Fig. 3AB). However, for a ramped increase in phosphatase the post-translational increase in σ^B is limited by the ramp rate of phosphatase increase which allows RsbW to catch up earlier and terminate the σ^B pulse thereby decreasing the pulse amplitude. To test this, we

varied the degradation rate and proportionally changed the rate of transcription of the σ^B operon to ensure that the total concentrations of σ^B, RsbW and RsbV are kept fixed (Fig. 3CD). Our simulations showed that the dependence of pulse amplitudes on ramp duration was indeed sensitive to the degradation rate (Fig. 3EF). This suggests that the timescale separation between the post-translational and transcriptional responses is in fact the basis of ramp rate encoding into pulse amplitudes.

The design of the σ^B network enables it to compete with σ^A for RNA polymerase

The results thus far indicate that σ^B network functions in the negative feedback regime where increase in the operon expression decreases σ^B activity. Negative feedback loops have been shown to increase the robustness of the system to perturbations. We therefore decided to investigate how the σ^B network design affects its performance when there is competition for RNA polymerase from other sigma factors like the housekeeping sigma factor σ^A. Since σ^A has a much higher affinity for RNA polymerase (18), a small increase in σ^A can dramatically increase the amount of σ^B necessary to activate the transcription of the σ^B regulon. Thus, changes in σ^A can alter the input-output relationship of a stress-response sigma factor like σ^B (Fig. S4AB) and thereby adversely affect the survival of cells under stress.

To understand how the σ^B network handles competition for RNA polymerase, we expanded our model to explicitly include σ^A, RNA polymerase (RNApol) and σ–RNApol complexes (Fig. 4A). Since post-translational reactions only depend on the concentrations of σ^B operon components and phosphatase, inclusion of σ^A did not change the post-translational function relating free σ^B to B_T and P_T. In contrast, looking at the transcription function, our model showed that an increase in σ^A decreased the 'effective affinity' of σ^B for RNApol and as a result, i.e. higher levels of free σ^B are necessary to achieve the same production rate of B_T or σ^B target genes.

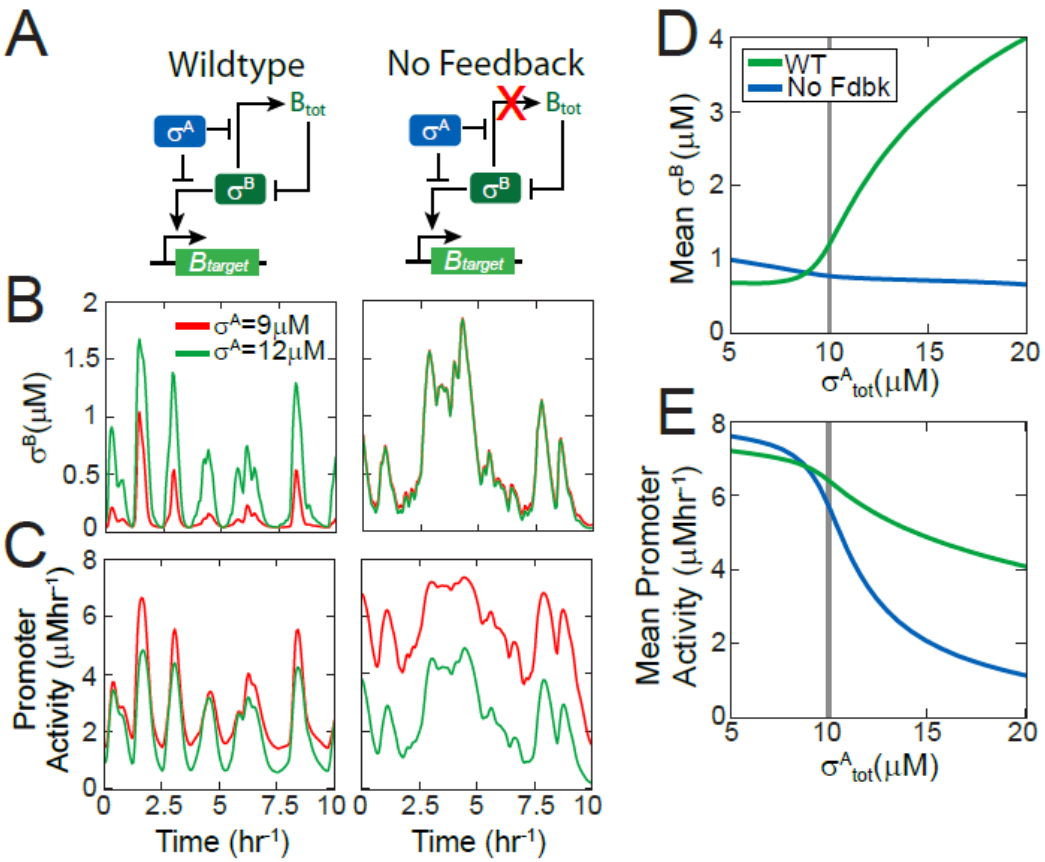

Figure 4. Negative feedback insulates the σ^B response from competition with housekeeping sigma factor σ^A. A. Simplified network diagrams of stress sigma factor σ^B competing with housekeeping sigma factor σ^A for RNA polymerase. In all cases, a σ^B phosphatase controls the stress-signal driven activation of σ^B. **B.** Trajectories of free σ^B response to stochastic phosphatase input for both networks at two different levels of σ^A (σ^A = 9μM-low competition for RNA polymerase; σ^A = 12μM-high competition for RNA polymerase). **C.** Output trajectories of σ^B target promoter activity in response to stochastic phosphatase input for all three networks at two different levels of σ^A. **D, E.** Mean free σ^B concentration (D) and mean σ^B target promoter activity (E) as a function of σ^A for both networks at fixed mean phosphatase (mean P_T = 0.5 μM). Gray vertical line shows the total RNA polymerase level which was fixed at 10 μM.

Next we examined the full model response, including both the transcriptional and post-translational components to changes in σ^A in the presence of energy stress signal, i.e. stochastically fluctuating RsbQP phosphatase levels. Our simulations showed that phosphatase bursts lead to pulses of free σ^B and σ^B target promoter activity (Fig. 4BC) similar to the results in Fig. 2. The pulsatile σ^B response is present since the full system still includes a negative interaction between σ^B and B_T (Fig. 4A). Notably our results also

showed that the pulse amplitudes of σ^B target promoter activity are not affected by ~30% increase in σ^A (Fig. 4C).

The surprising insensitivity of the phosphatase-σ^B target dose-response to RNApol competition is the result of the ultrasensitive negative feedback between σ^B and B_T. Due to the ultrasensitivity of this feedback, a small decrease in B_T resulting from the increase in σ^A causes a large increase in σ^B pulse amplitude (Fig. 4B, D). This increased amplitude compensates for the increased competition for RNApol and insulates the network from perturbations (Fig. 4DE).

To test the importance of the negative feedback in insulating the network we compared the response of the wildtype network to a mutant network wherein the σ^B operon is constitutive rather than σ^B dependent (Fig. 4A). Consequently this network lacks any feedback between σ^B and B_T. As shown in Fig. 4BD, the free σ^B response of the no feedback network response does not pulse and an increase in σ^A did not affect this response. This is expected since B_T and thus free σ^B are independent of σ^A which only affects the expression of σ^B targets in this network (Fig. 4A). Without an increase in free σ^B, the increased competition for RNApol at higher σ^A results in reduced σ^B target promoter activity in this network (Fig. 4CE). Notably a positive feedback network design is similarly incapable of increasing free σ^B in response to an increase in σ^A (Fig. S4CDE). Thus fluctuations in σ^A can lead to unwanted variability in the σ^B stress-response of these alternative network designs. In contrast, the wildtype σ^B network with its ultrasensitive negative feedback design is ideally designed to compensate for competition effects (Fig. 4DE).

Negative feedback designs of stress-response sigma factor networks minimizes interference

The negative feedback design of the network discussed here is not unique to σ^B. Several stress sigma factors in *B. subtilis* as well as other bacteria are regulated in similar fashion (3, 13, 27-30). For example σ^W, a sigma factor in *B. subtilis* that controls the response to alkaline shock (31) is co-transcribed with its anti-sigma factor RsiW. In the absence of stress, RsiW sequesters σ^W in an inactive complex. σ^W is activated by stress signals which trigger the cleavage and degradation of RsiW thereby releasing and activating σ^W target expression (32). Although it is unknown whether the σ^W network functions in a negative feedback regime similar to σ^B or if it pulses, it is possible for this network to exhibit these design properties. If RsiW is expressed in stoichiometric excess of its binding partner σ^W from the σ^W-regulated operon which they share (33), then similar to the σ^B network, σ^W would operate in a negative feedback regime.

To determine if negative feedback control offers any advantages when multiple stress sigma factors are active, we built a new model that includes three sigma factors: σ^B, σ^W and σ^A. Anti-sigma factors RsbW (RsiW) and other details of post-translational regulation were excluded for simplicity. Instead the regulation of free σ^B and σ^W was modeled with simplified identical versions of the negative feedback design of the σ^B network (Fig. S5A). Under this simplification, free σ^B and free σ^W are non-monotonically functions of B_T (total σ^B) and W_T (total σ^W) respectively. These non-monotonic functions are qualitatively similar to the post-translational response function shown in Fig. 1C and depend on a signaling proteins P_B (for σ^B) and P_W (for σ^W). Following the previous section, this model explicitly includes σ^A, RNA polymerase (RNApol) and σ–RNApol complexes such that the transcriptional responses for both σ^B and σ^W depend on σ^A and RNApol concentrations (see Supplementary Text). Concentrations of RNApol and σ^A were chosen to ensure that amount of RNApol is insufficient to bind to all sigma-factors at the same time. All other parameters of the simplified model were chosen to approximately match the full σ^B network model and ensure that both σ^B and σ^W operate in the negative feedback regime. Consequently for the chosen parameters this simplified model acts like our detailed model and responds to step increases in the signaling protein P_B (or P_W) by producing a pulse of σ^B (or σ^W) activity (Fig. S5CD).

We used this simple model to study the response when cells are simultaneously exposed to multiple stresses creating competition for RNApol. Our results showed that similar to effect of increasing σ^A (Fig. S4AB), increased availability of one stress sigma factor leads to competition for RNA polymerase and as a result reduces activity of the other stress sigma factor (Fig. S5EF). However, our results also showed that when negative feedbacks are present, surprisingly, increasing the stress signal for one sigma factor also led to the activation of the other sigma factor. For example, increasing P_B while keeping P_W fixed leads to an increase in free σ^B but also results in a smaller increase in free σ^W (Fig. 5C). This response can be explained by the ultrasensitive negative feedback loops controlling the stress sigma factors. Increase in free σ^B by P_B leads to increased competition for RNApol resulting in a decrease in production of W_T. But since σ^W is regulated by a negative feedback, a decrease in W_T actually frees up more σ^W thereby insulating σ^W target activity from the effects of RNApol competition (Fig. 5E). Similarly the dynamic response of the stress sigma factors is also insulated from competition and an increase in fixed P_W levels increases the pulse amplitude of σ^B in response to step changes in P_B (Fig. S5A-D).

Thus the two stress sigma factors are able to function simultaneously despite the scarcity of RNApol. This cross-talk between stress sigma factors becomes clearer when we track the changes in σ–RNApol complexes as a function of stress signal P_B. As P_B increases, more free σ^B becomes available and binds to RNApol (Fig. 5G). However

this RNApol must be accounted for by the RNApol lost by the other operating sigma factors σ^W and σ^A. Comparing the contributions of each sigma factor shows that despite the fact that σ^A has a much higher affinity for RNApol, most of the RNApol in the σ^B-RNApol complex is drawn from the σ^A-RNApol pool rather than σ^W-RNApol pool (Fig. 5G). Thus the negative feedback design allows stress sigma factors to cooperate and avoid competing with each other at the expense of the housekeeping sigma factor σ^A.

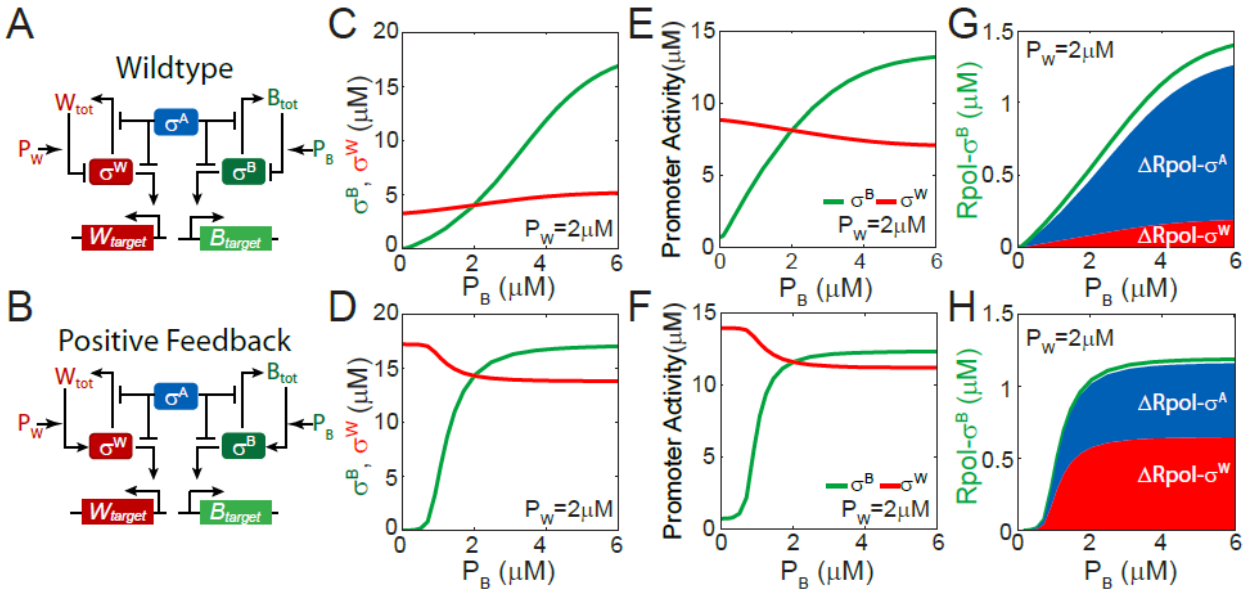

Figure 5. Negative feedback minimizes competition between stress σ factors for RNA polymerase. A,B. Simplified network diagrams of stress sigma factors σ^B and σ^W and housekeeping sigma factor σ^A competing with each other for RNA polymerase. σ^B and σ^W activities are regulated by negative and positive feedbacks in (A) and (B) respectively. In both cases, signaling proteins P_B and P_W control the stress-signal driven activation of σ^B and σ^W respectively. **C, D.** Dependence of free σ^B and σ^W levels on P_B at fixed P_W (= 2μM). In the wildtype negative feedback system (C), increase in σ^B phosphatase leads to an increase in both free σ^B (green curve) and free σ^W (red curve). In the positive feedback system (D), increase in σ^B phosphatase leads to an increase in free σ^B (green curve) and a decrease in free σ^W (red curve). **E, F.** σ^B and σ^W target promoter activities as a function of P_B at fixed P_W in the wildtype negative feedback system (E), and the positive feedback system (F). **G, H.** RNA polymerase bound σ^B (Rpol-σ^B) as a function of P_B at fixed P_W in the wildtype negative feedback system (G) and the positive feedback system (H). Increase in σ^B phosphatase (P_B) leads to an increase in Rpol-σ^B (green curve) and corresponding decreases ΔRpol-σ^W in Rpol-σ^W (red area) and ΔRpol-σ^A in Rpol-σ^A (blue area).

The role of the negative feedback in producing this cross-talk response becomes clear when we compare the response of a mutant network that has positive feedback loops between σ^B and B_T and σ^W and W_T. As shown in Fig. 5D, unlike the wildtype response, increase in P_B and the resulting increase in free σ^B decreases the free σ^W in the positive

feedback network. As a result of the increased competition for RNApol and the decreased free σ^W, σ^W target promoter activity in this network decreases as a function of P_B (Fig. 5F). Moreover comparing changes in σ–RNApol complexes as a function of stress signal P_B we find that most of the RNApol in the σ^B-RNApol complex is drawn from the σ^W-RNApol pool rather than σ^A-RNApol pool (Fig. 5H). Thus the negative feedback designs are not only essential for stress sigma factors to tolerate competition from σ^A, but also necessary for them to cooperate and avoid competing with each other when the cell is simultaneously exposed to multiple types of stresses.

Discussion

Taken together, our results show how the design of the σ^B network includes an implicit ultrasensitive negative feedback that plays multiple functional roles. This design enables pulsatile activation of σ^B in response to energy stress and rate-sensitivity to increases in environmental stress. Moreover, we show that the same design feature allows the network to effectively compete with house-keeping and other alternative sigma factors for RNA polymerase core.

Prompted by recent observations of the highly dynamic pulsatile response of the σ^B network (ref), we have developed a new mathematical model that reproduces all reported features of the response including pulsatile activation in response to stress. Our model avoids making ad hoc simplifications and instead captures all the known molecular details of the network. By decoupling the post-translational and transcriptional responses in our model we were able to derive a simplified view of the network that illustrates how the pulsatile response is mechanistically based on the ultrasensitive negative feedback in the network. Using this method we identified the relative stoichiometry of σ^B, RsbW and RsbV synthesis rates as the most critical design property, which by controlling the post-translational response determines the sign of the feedback in the network as well as all qualitative features of the network response. This highlights how ignoring non-transcriptional interactions and focusing on transcriptional regulatory interactions alone can be misleading when trying to identify or characterize network motifs. Notably, recent analyses of networks like bacterial two-component systems (34) and the sporulation phosphorelay (35) have similarly shown how the sign of feedback in these networks depends critically on their post-translational design.

The decoupling of the post-translational and transcriptional response greatly facilitated the identification of critical design features despite the complexity of the network. This separation greatly reduces the dimensionality of the dynamical system by enabling an independent input–output analysis for the two modules. Similar methods have been applied to deduce core functional properties in a variety of studies and model systems

(36-38). Interestingly our analysis revealed that the post-translational and transcriptional module structures of the network and the phosphorelay controlling *B. subtilis* sporulation are remarkably similar (35). Despite the differences in molecular details, both networks possess a non-monotonic post-translational dependence of the active transcription factor on the concentration of the total transcription factor. Combining this response with the transcriptional feedback produces an ultrasensitive negative feedback in both networks. The relevance of these similarities is evidenced by the fact that both networks produce dynamically similar pulsatile responses even though they are activated by entirely different stimuli.

We further showed that energy stress can control σ^B pulses frequency by modulating the size of stochastic bursts of energy stress phosphatase. This result raises a question about whether pulsatile σ^B response can achieve proportional expression of downstream genes, as was previously suggested (14, 39). This proportional control requires the distribution of pulse amplitudes to remain fixed even as stress levels increase. However under the burst size encoding strategy, pulse amplitude distributions change as stress levels increase thereby negating the efficacy of a pulsed response in producing proportional expression of downstream genes. The functional significance of pulsatile response may instead lie in its ability to encode the rate of environmental stress increase. Our model showed that this rate encoding follows from the timescale separation between the fast post-translational and the slow transcriptional responses in the network. As a result cells are able to encode the rate of stress increase into σ^B pulses. This rate responsiveness is only possible with adaptive pulsatile responses and thus may explain the need for σ^B pulsing to control the general stress response.

We also used our model to understand the response when placed in the larger context of other sigma factor networks and competition for RNA polymerase. Our results show how the network design is uniquely suited to insulating its response from RNA polymerase competition from the housekeeping sigma factor. Finally we demonstrate how ultrasensitive negative feedback, a ubiquitous feature of stress sigma factor regulation enables different stress sigma factors to operate simultaneously without inhibiting each other. These results are relevant not only for understanding the stress response of bacteria but also increasingly for the design of synthetic circuits. The movement towards the construction of larger genetic circuits has produced numerous recent designs that include multiple independent modules that rely on shared resources or actuators to function (40-42). Our results highlight how competition between modules for shared resources can significantly affect the performance of these synthetic circuits. Further, inspired by the design of naturally occurring stress sigma factor network we provide new design rules, that can improve the performance and robustness of the synthetic networks.

Methods

Mathematical model of the σ^B network

Our mathematical model of σ^B network is based on a previous model proposed in (16). This ODE-based model explicitly includes all known molecular species, post-translational reactions and the transcriptional regulation of the σ^B operon by σ^B. The stress signals were assumed to control the concentrations of stress phosphatases RsbTU and RsbQP. For RsbQP, energy stress was assumed to regulate the transcription rate of the phosphatase and the phosphatase concentration was assumed to be subject to stochastic fluctuations resulting from gene expression noise. In contrast, RsbTU concentration is regulated by environmental stress post-translationally, consequently RsbTU concentration was assumed to be stress-dependent but not subject to stochastic fluctuations. The details of all biochemical reactions in the model and the corresponding differential equations are described in the Supplementary Text. All model parameters are summarized in Table S1.

To study the effects of competition for RNA polymerase, the σ^B network model was expanded to include reactions for σ^A, RNA polymerase (RNApol) and σ–RNApol binding (see Supplementary Text). To investigate the competition between σ^B, σ^W and σ^A, we used a phenomenological non-monotonic function to model the post-translational regulation of stress sigma factors (σ^B and σ^W; see Supplementary Text for details).

Calculation of steady state post-translational and transcriptional responses

The decoupled transcriptional and post-translational responses of the network at steady state were calculated using the MATLAB bifurcation package MATCONT. The post-translational response $\sigma^B = F_P(B_T,P_T)$, was calculated by varying the rate of operon transcription while keeping the component synthesis rates (λ_W, λ_V) and the total phosphatase concentration (P_T) fixed. Similarly, the transcriptional response $B_T = F_T(\sigma^B)$, was calculated by varying the free σ^B concentration as an independent variable to calculate the total concentrations of σ^B, RsbW and RsbV.

Simulations

In the deterministic set-up, the system of differential equations was solved using standard *ode15s* solver in MATLAB. For stochastic simulations the time-varying total phosphatase level P_T (= P + V_PP) was pre-computed using a gamma distributed Ornstein-Uhlenbeck process as in (14). This gamma distributed Ornstein-Uhlenbeck process permits independent modulation of mean burst size (*b*) and frequency (*a*) (43). For each phosphatase level, 50 simulations were performed each lasting 10 hours.

Pulses were detected by examining local maxima and minima of the simulated trajectories, and subsequently this information was used to compute pulse statistics for amplitude and frequency.

Acknowledgments

The research was supported by NIH grants GM 096189 to OAI. The authors are grateful to James Locke for sharing raw data from Ref. (14) and Chet Price for feedback on the manuscript.

References

1. Nichols RJ*, et al.* (2011) Phenotypic landscape of a bacterial cell. *Cell* 144(1):143-156.
2. Nicolas P*, et al.* (2012) Condition-dependent transcriptome reveals high-level regulatory architecture in Bacillus subtilis. *Science* 335(6072):1103-1106.
3. Helmann JD (2002) The extracytoplasmic function (ECF) sigma factors. *Adv Microb Physiol* 46:47-110.
4. Gruber TM & Gross CA (2003) Multiple sigma subunits and the partitioning of bacterial transcription space. *Annu Rev Microbiol* 57:441-466.
5. Osterberg S, del Peso-Santos T, & Shingler V (2011) Regulation of alternative sigma factor use. *Annu Rev Microbiol* 65:37-55.
6. Hecker M, Pane-Farre J, & Volker U (2007) SigB-dependent general stress response in Bacillus subtilis and related gram-positive bacteria. *Annu Rev Microbiol* 61:215-236.
7. Dufour A & Haldenwang WG (1994) Interactions between a Bacillus subtilis anti-sigma factor (RsbW) and its antagonist (RsbV). *J Bacteriol* 176(7):1813-1820.
8. Kang CM, Brody MS, Akbar S, Yang X, & Price CW (1996) Homologous pairs of regulatory proteins control activity of Bacillus subtilis transcription factor sigma(b) in response to environmental stress. *J Bacteriol* 178(13):3846-3853.
9. Vijay K, Brody MS, Fredlund E, & Price CW (2000) A PP2C phosphatase containing a PAS domain is required to convey signals of energy stress to the sigmaB transcription factor of Bacillus subtilis. *Mol Microbiol* 35(1):180-188.
10. Voelker U, Voelker A, & Haldenwang WG (1996) Reactivation of the Bacillus subtilis anti-sigma B antagonist, RsbV, by stress- or starvation-induced phosphatase activities. *J Bacteriol* 178(18):5456-5463.
11. Yang X, Kang CM, Brody MS, & Price CW (1996) Opposing pairs of serine protein kinases and phosphatases transmit signals of environmental stress to activate a bacterial transcription factor. *Genes Dev* 10(18):2265-2275.
12. Alper S, Dufour A, Garsin DA, Duncan L, & Losick R (1996) Role of adenosine nucleotides in the regulation of a stress-response transcription factor in Bacillus subtilis. *J Mol Biol* 260(2):165-177.
13. Haldenwang WG (1995) The sigma factors of Bacillus subtilis. *Microbiol Rev* 59(1):1-30.
14. Locke JC, Young JW, Fontes M, Hernandez Jimenez MJ, & Elowitz MB (2011) Stochastic pulse regulation in bacterial stress response. *Science* 334(6054):366-369.
15. Young JW, Locke JC, & Elowitz MB (2013) Rate of environmental change determines stress response specificity. *Proc Natl Acad Sci U S A* 110(10):4140-4145.

16. Igoshin OA, Brody MS, Price CW, & Savageau MA (2007) Distinctive topologies of partner-switching signaling networks correlate with their physiological roles. *J Mol Biol* 369(5):1333-1352.
17. Grigorova IL, Phleger NJ, Mutalik VK, & Gross CA (2006) Insights into transcriptional regulation and sigma competition from an equilibrium model of RNA polymerase binding to DNA. *Proc Natl Acad Sci U S A* 103(14):5332-5337.
18. Rollenhagen C*, et al.* (2003) Binding of sigma(A) and sigma(B) to core RNA polymerase after environmental stress in Bacillus subtilis. *J Bacteriol* 185(1):35-40.
19. Delumeau O, Lewis RJ, & Yudkin MD (2002) Protein-protein interactions that regulate the energy stress activation of sigma(B) in Bacillus subtilis. *J Bacteriol* 184(20):5583-5589.
20. Ma W, Trusina A, El-Samad H, Lim WA, & Tang C (2009) Defining network topologies that can achieve biochemical adaptation. *Cell* 138(4):760-773.
21. Cai L, Friedman N, & Xie XS (2006) Stochastic protein expression in individual cells at the single molecule level. *Nature* 440(7082):358-362.
22. Friedman N, Cai L, & Xie XS (2006) Linking stochastic dynamics to population distribution: an analytical framework of gene expression. *Phys Rev Lett* 97(16):168302.
23. Taniguchi Y*, et al.* (2010) Quantifying E. coli proteome and transcriptome with single-molecule sensitivity in single cells. *Science* 329(5991):533-538.
24. Dufour A, Voelker U, Voelker A, & Haldenwang WG (1996) Relative levels and fractionation properties of Bacillus subtilis sigma(B) and its regulators during balanced growth and stress. *J Bacteriol* 178(13):3701-3709 sigma.
25. Kang CM, Vijay K, & Price CW (1998) Serine kinase activity of a Bacillus subtilis switch protein is required to transduce environmental stress signals but not to activate its target PP2C phosphatase. *Mol Microbiol* 30(1):189-196.
26. Marles-Wright J*, et al.* (2008) Molecular architecture of the "stressosome," a signal integration and transduction hub. *Science* 322(5898):92-96.
27. Brooks BE & Buchanan SK (2008) Signaling mechanisms for activation of extracytoplasmic function (ECF) sigma factors. *Biochim Biophys Acta* 1778(9):1930-1945.
28. Kingston AW, Liao X, & Helmann JD (2013) Contributions of the sigma(W) , sigma(M) and sigma(X) regulons to the lantibiotic resistome of Bacillus subtilis. *Mol Microbiol* 90(3):502-518.
29. Mascher T (2013) Signaling diversity and evolution of extracytoplasmic function (ECF) sigma factors. *Curr Opin Microbiol* 16(2):148-155.
30. Yoshimura M, Asai K, Sadaie Y, & Yoshikawa H (2004) Interaction of Bacillus subtilis extracytoplasmic function (ECF) sigma factors with the N-terminal regions of their potential anti-sigma factors. *Microbiology* 150(Pt 3):591-599.
31. Wiegert T, Homuth G, Versteeg S, & Schumann W (2001) Alkaline shock induces the Bacillus subtilis sigma(W) regulon. *Mol Microbiol* 41(1):59-71.
32. Heinrich J, Hein K, & Wiegert T (2009) Two proteolytic modules are involved in regulated intramembrane proteolysis of Bacillus subtilis RsiW. *Mol Microbiol* 74(6):1412-1426.
33. Huang X, Gaballa A, Cao M, & Helmann JD (1999) Identification of target promoters for the Bacillus subtilis extracytoplasmic function sigma factor, sigma W. *Mol Microbiol* 31(1):361-371.
34. Ray JC & Igoshin OA (2010) Adaptable functionality of transcriptional feedback in bacterial two-component systems. *PLoS Comput Biol* 6(2):e1000676.
35. Narula J*, et al.* (2015) Chromosomal Arrangement of Phosphorelay Genes Couples Sporulation and DNA Replication. *Cell* 162(2):328-337.
36. Miyashiro T & Goulian M (2008) High stimulus unmasks positive feedback in an autoregulated bacterial signaling circuit. *Proc Natl Acad Sci U S A* 105(45):17457-17462.

37. Tiwari A, Balazsi G, Gennaro ML, & Igoshin OA (2010) The interplay of multiple feedback loops with post-translational kinetics results in bistability of mycobacterial stress response. *Phys Biol* 7(3):036005.
38. Tiwari A, Ray JC, Narula J, & Igoshin OA (2011) Bistable responses in bacterial genetic networks: designs and dynamical consequences. *Math Biosci* 231(1):76-89.
39. Levine JH, Lin Y, & Elowitz MB (2013) Functional roles of pulsing in genetic circuits. *Science* 342(6163):1193-1200.
40. Cookson NA*, et al.* (2011) Queueing up for enzymatic processing: correlated signaling through coupled degradation. *Mol Syst Biol* 7:561.
41. Nielsen AA & Voigt CA (2014) Multi-input CRISPR/Cas genetic circuits that interface host regulatory networks. *Mol Syst Biol* 10:763.
42. Segall-Shapiro TH, Meyer AJ, Ellington AD, Sontag ED, & Voigt CA (2014) A 'resource allocator' for transcription based on a highly fragmented T7 RNA polymerase. *Mol Syst Biol* 10:742.
43. Barndorff-Nielsen OE & Shephard N (2001) Non-Gaussian Ornstein-Uhlenbeck-based models and some of their uses in financial economics. *J R Stat Soc B* 63:167-207.